Combined optical fluorescence microscopy and X-ray tomography reveals substructures in cell nuclei in 3D: supplement

ANDREW WITTMEIER,[1] MARTEN BERNHARDT,[1] ANNA-LENA ROBISCH,[1] CHIARA CASSINI,[1,2] MARKUS OSTERHOFF,[1] TIM SALDITT,[1,2] ⓘD AND SARAH KÖSTER[1,2,*] ⓘD

[1]*Institute for X-Ray Physics, University of Göttingen, Friedrich-Hund-Platz 1, 37077 Göttingen, Germany*
[2]*Cluster of Excellence "Multiscale Bioimaging: from Molecular Machines to Networks of Excitable Cells" (MBExC), University of Göttingen, Germany*
[*]*Sarah.Koester@phys.uni-goettingen.de*

Supplementary Information for:
Combined optical fluorescence microscopy and X-ray tomography reveals substructures in cell nuclei in 3D

ANDREW WITTMEIER,[1] MARTEN BERNHARDT,[1] ANNA-LENA ROBISCH,[1] CHIARA CASSINI,[1,2] MARKUS OSTERHOFF,[1] TIM SALDITT,[1,2] SARAH KÖSTER,[1,2,*]

[1] *Institute for X-Ray Physics, University of Göttingen, Friedrich-Hund-Platz 1, 37077 Göttingen, Germany*
[2] *Cluster of Excellence "Multiscale Bioimaging: from Molecular Machines to Networks of Excitable Cells" (MBExC), University of Göttingen, Germany*
[*] *Corresponding email: sarah.koester@phys.uni-goettingen.de*

S1.   Center plane determination

Throughout the main text, the correlation between the tomography and confocal data sets is based on the assumption that the cell nucleus is approximately ellipsoidal in shape and thus contains the most biological material in the center plane as it has the largest area.

To determine the center micrograph of the confocal z-stack, all detected counts for each micrograph are summed. Figure S1a shows the distribution of integrated counts. The micrograph with the largest integrated count (Fig. S1b) defines the center plane of the confocal z-stack. To determine the center slice of the tomographic volume (voxel side length: 65.1 nm), a slice in which the cell nucleus is visually well-defined (Fig. S1c) is first chosen. Next, a region-of-interest (ROI) is manually defined around the nucleus (red, Fig. S1c). A zoom-in of the ROI is shown in Fig. S1d. Next, all phase shift values bound by the ROI are summed for each slice of the tomographic volume (Fig. S1e). As a consequence of nucleus' perimeter not being visually well-defined for all slices the ROI is intentionally larger than the nucleus, thus ensuring that a smaller integrated phase value for the slices that contain more material, i.e., the center of the nucleus, is achieved. The slice with the smallest integrated phase shift, corresponding to the slice with the largest amount of biological matter, defines the center slice of the tomographic volume (Fig. S1f). The black box in Fig. S1f defines a ROI used for background-correction. Following the determination of the center slice, 112 slices, of the possible 2048, are used to create 28 260.4 nm-thick slices, i.e., the number of confocal micrographs. Each 260.4 nm-thick slice is created by adding four 65.1 nm-thick slices in a pixel-wise manner. The 112 slices used for this rendering process are selected with respect to the center slice, i.e., the 56 slices below and 55 slices above. Thus, slice 1132 (Fig. S1f) is one of four slices comprising the 260.4 nm-thick slice shown in Fig. S1g. The 260.4 nm-thick slices are used for subsequent data analysis. Slice 18, representing the same z-plane as the center confocal micrograph (Fig. S1b), is shown in Fig. S1g.

Next, we spatially correlate the tomography and confocal data sets. Towards this end, a logic mask is manually drawn around the nucleus of slice 18 (Fig. S1h) and the center confocal micrograph (Fig. S1i). The center-of-mass and angular orientation of both logic masks are determined. The logic mask of tomographic slice 18 (Fig. S1h) is subsequently rotated, translated and resized such that it has the same angular orientation, center-of-mass and pixel size as both the center confocal micrograph (Fig. S1b) and its corresponding logic mask (Fig. S1i). (Note subfigures h) and i) only serve as a visual aid to the reader.) All 28 slices undergo identical transformation changes as the logic mask of slice 18. Figure S1j shows the same slice shown in Fig. S1g only resized and rotated. All rotated and resized slices are subsequently cropped such

that they have the same field-of-view as the confocal micrographs. Figure S1k shows a cropped and enlarged version of Fig. S1j. To verify that the center plane of the tomography and confocal volumes represent the same plane of the nucleus, the pixel values are summed for each of the 28 tomography slices. Figure S1l shows the distribution of the integrated electron density counts. Slice 18 has the largest integrated count value and is in agreement with the center micrograph of the confocal z-stack, micrograph 18 (Fig. S1a,b).
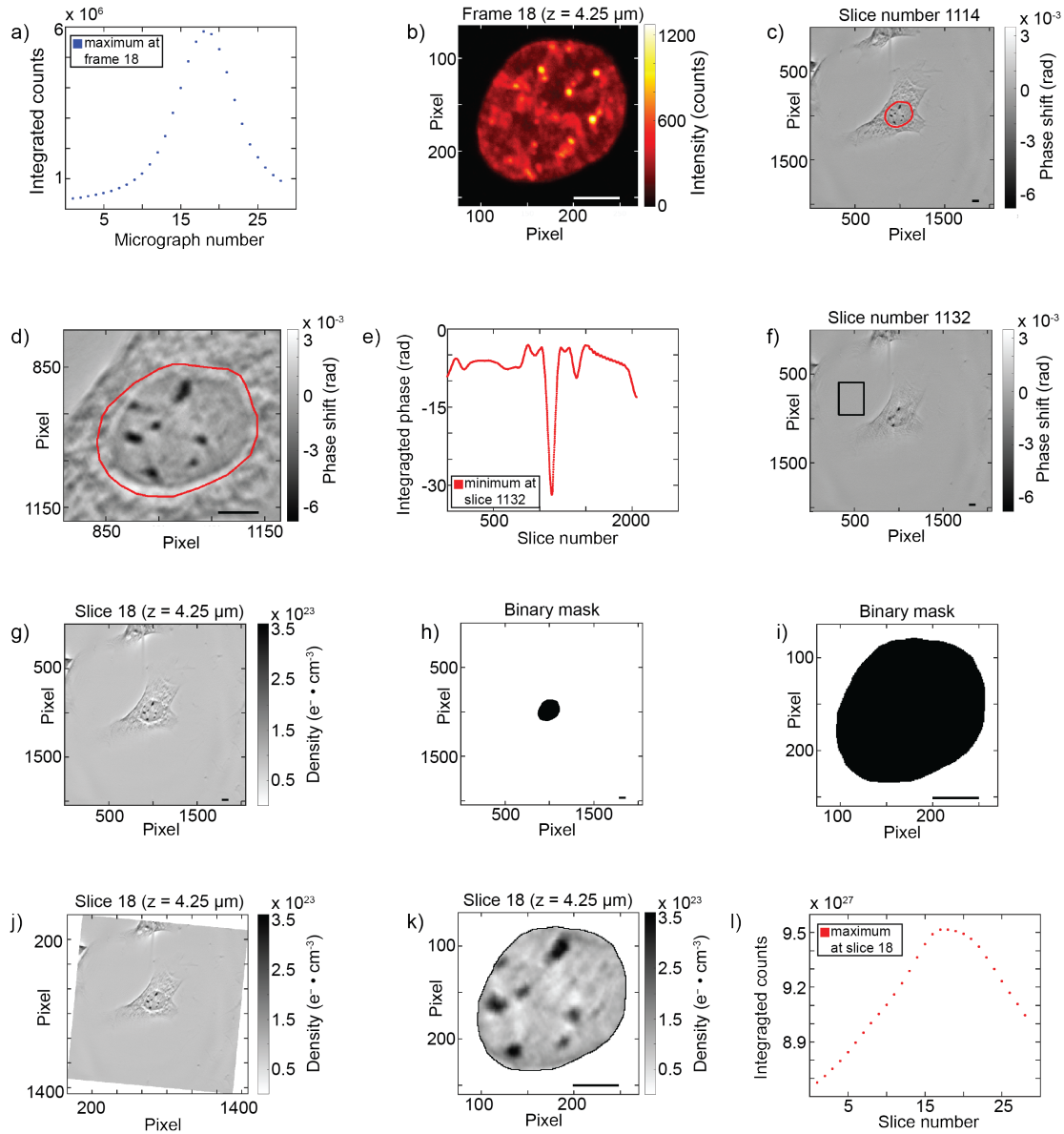
Fig. S1. a) Distribution of integrated photon counts for micrographs comprising the confocal *z*-stack of nucleus 1. b) The center micrograph of the confocal *z*-stack. c) A tomographic slice for which the nucleus is visually well-defined. The ROI around the nucleus is shown in red. d) Zoom-in of the ROI shown in c). For each slice the reconstructed phase shift values bound by the ROI of the nucleus are summed. e) Distribution of integrated phase shift values. f) The center slice of the tomographic volume. The black box defines the region used for background correction. g) A 260.4 nm-thick slice. This slice represents the same plane of the nucleus shown in subfigure b). h) Logic mask of the nucleus shown in subfigure g). i) Logic mask of the nucleus shown in subfigure b). j) Rotated and resized version of subfugure g). This subfigure has the same angular orientation and pixel size of subfigure b). k) Cropped and enlarged version of subfigure j). This subfigure has the same field-of-view shown in subfigure b). l) Distribution of the integrated electron density of each of the 28 resized and rotated tomographic slices. All scale bars are 5 μm.

S2. Visible light phase contrast microscopy

Figure S2 shows epifluorescence images of cell nuclei (red) overlaid on visible light phase contrast images of lyophilized NIH-3T3 cells adhered to a silicon-rich nitride membrane. Images are acquired using an inverted microscope (IX81, Olympus, Hamburg, Germany) equipped with a Retiga 6000 Monochrome camera (QImaging, Tucson, AZ, USA) and a 20× phase contrast objective (UCPlanFLN, NA = 0.7; Olympus).
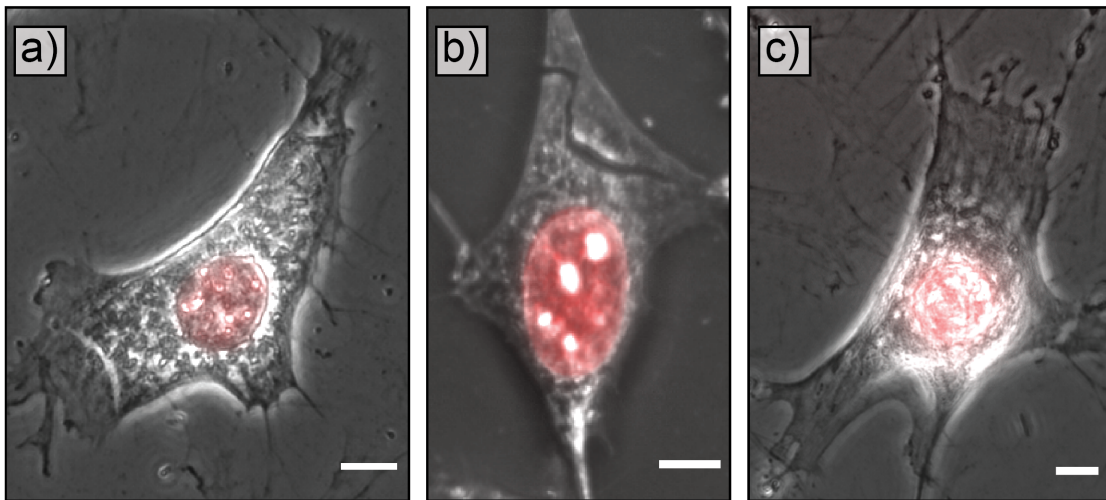

Fig. S2. Epifluorescence images of cell nuclei (red) overlaid on visible light phase contrast images of lyophilized NIH-3T3 cells adhered to a silicon-rich nitride membrane. Cells corresponding to nucleus 1, 2 and 3 of the main text are shown in a), b), and c), respectively. All scale bars are $10\,\mu m$.

S3. Image segmentation

For each of the three biological cells, the segmentation of heterochromatin, euchromatin and pericentric heterochromatin foci (PHFs) is based on the following approach: Using the center confocal micrograph (Fig. S3a, Fig. S1b), an intensity-value threshold is determined, which, through visual inspection, segments the bright, globular regions we interpret as PHFs (Fig. S3b). To aid the visualization of segmented PHFs the colormap of Fig. S3b is inverted. To segment the heterochromatin and euchromatin, a second intensity-value threshold is determined also using the center confocal micrograph: The threshold is set in such a way that the mean intensity of one segmented region (Fig. S3c) is 2-fold larger than the mean intensity of remaining pixels (Fig. S3d), thus defining the segmentation of heterochromatin and euchromatin, respectively. Note that the segmented PHFs are first subtracted from the confocal micrograph prior to the segmentation of heterochromatin and euchromatin. The thresholds used to segment the heterochromatin, euchromatin and PHFs in the center confocal micrograph are kept constant and applied to each micrograph of a confocal z-stack. For each micrograph of the confocal stack a unique logic mask is created which maps the spatial distribution of each substructure. Figure S3e shows the logic mask of the segmented PHFs (yellow), heterochromatin (orange) and euchromatin (blue) of the micrograph shown in Fig. S3a. Figure S3a and e are also shown in Fig. 3a and b of the main text, respectively.

The segmentation of nucleoli follows a similar approach: Using the center tomographic slice (Fig. S3f, Fig. S1k), an intensity value threshold is determined which, through visual inspection, segments the dense, globular regions which we interpret as nucleoli (Fig. S3g). This threshold is kept constant and applied to every slice comprising the tomographic stack. For each tomographic slice a logic mask is created which separates the spatial distribution of the nucleoli and remaining biological material. Figure S3h shows the segmented nucleoli (purple) and remaining biological material (cyan) of the tomographic slice shown in Fig. S3f. Figure S3f and h are also shown in Fig. 5a and b of the main text, respectively.
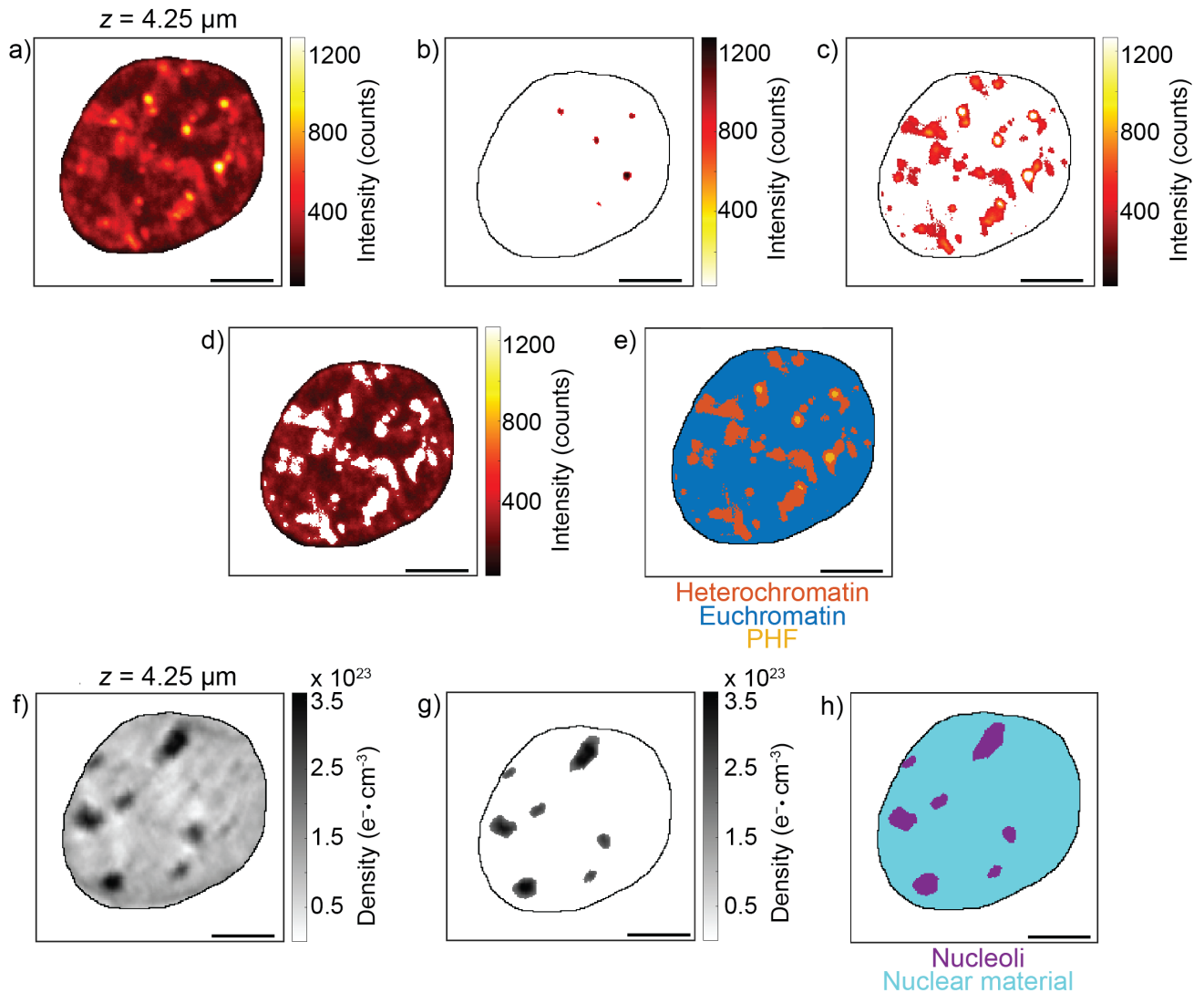
Fig. S3. The example in this figure corresponds to nucleus 1, as presented throughout the main text. a) Center confocal micrograph of the stack shown in Fig. 2a in the main text. b) Segmented PHFs. To aid the visualization of segmented PHFs the color axis is inverted. c) Segmented heterochromatin. d) Segmented euchromatin. e) Logic mask of the segmented PHFs (yellow), heterochromatin (orange) and euchromatin (blue). f) Center slice of the tomographic volume shown in Fig. 5a in the main text. g) Segmented nucleoli of subfigure f). h) Logic mask of the segmented nucleoli (purple) and remaining biological material (cyan). All scale bars are 5 μm.

S4. Distributions of measured quantities

For every slice of the confocal micrograph the percentage of intensity stemming from hete-
rochromatin is calculated (Fig. S4a). For every tomographic slice the percentage of its total
electron density stemming from nucleoli is calculated (Fig. S4b). Furthermore, the percentage
of heterochromatin that is inactive is calculated for every slice of the nucleus (Fig. S4c).
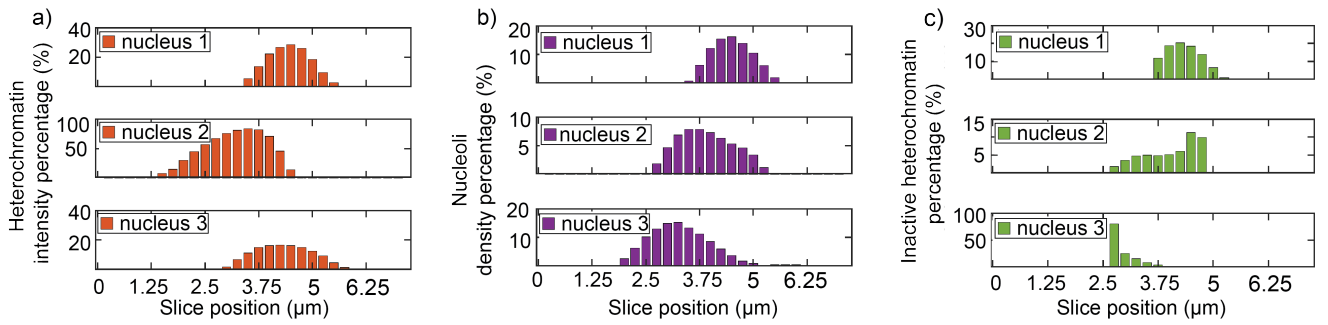

Fig. S4. a) Percentage of fluorescent intensity stemming from heterochromatin. b)
Percentage of the total electron density stemming from nucleoli. c) Percentage of
inactive heterochromatin.